Highly transparent and reproducible nanocrystalline ZnO and AZO thin films grown by room temperature pulsed-laser deposition on flexible Zeonor plastic substrates

*Saikumar Inguva [1], Rajani K. Vijayaraghavan [2], Enda McGlynn [1], Jean-Paul Mosnier [1, *]*

[1]School of Physical Sciences and National Centre for Plasma Science and Technology,

Dublin City University, Glasnevin, Dublin 9, Ireland.

[2]School of Electronic Engineering and National Centre for Plasma Science and Technology,

Dublin City University, Glasnevin, Dublin 9, Ireland.

*Jean-Paul.Mosnier@dcu.ie

KEYWORDS

ZnO and AZO thin films, Zeonor substrates, flexible plastic substrates, pulsed laser deposition, room temperature deposition.

ABSTRACT

Zeonor plastics are highly versatile due to exceptional optical and mechanical properties which make them the choice material in many novel applications. For potential use in flexible transparent optoelectronic applications, we have investigated Zeonor plastics as flexible substrates for the deposition of highly transparent ZnO and AZO thin films. Films were prepared by pulsed laser deposition at room temperature in oxygen ambient pressures of 75, 150 and 300 mTorr. The growth rate, surface morphology, hydrophobicity and the structural, optical and electrical properties of as-grown films with thicknesses ~ 65 nm - 420 nm were recorded for the three oxygen pressures. The growth rates were found to be highly linear both as a function of film thickness and oxygen pressure, indicating high reproducibility. All the films were optically smooth, hydrophobic and nanostructured with lateral grain shapes of ~ 150 nm wide. This was found compatible with the deposition of condensed nanoclusters, formed in the ablation plume, on a cold and amorphous substrate. Films were nanocrystalline (wurtzite structure), *c*-axis oriented, with average crystallite size ~ 22 nm for ZnO and ~ 16 nm for AZO. In-plane compressive stress values of 2-3 GPa for ZnO films and 0.5 GPa for AZO films were found. Films also displayed high transmission greater than 95 % in some cases, in the 400 – 800 nm wavelength range. The low temperature photoluminescence spectra of all the ZnO and AZO films showed intense near band edge emission. A considerable spread from semi-insulating to n-type conductive was observed for the films, with resistivity $\sim 10^3$ Ω cm and Hall mobility in 4 - 14 cm^2/V-s range, showing marked dependences on film thickness and oxygen pressure. Applications in the fields of microfluidic devices and flexible electronics for these ZnO and AZO films are suggested.

1. Introduction

Novel applications in flexible transparent electronics and optoelectronics, such as flat panel displays [1], solar cells [2], organic light emitting diodes [3] or thin film transistors [4,5] require the deposition of high-quality semiconductor oxide thin films on flexible, plastic instead of glass, substrates. This is because the mechanical properties (flexibility, low density, compactness, impact resistance) and generally the low-cost of most plastic materials [6,7] compare advantageously with those of glass. ZnO and ZnO:Al (AZO) are well-known semiconductor oxide materials for thin film deposition and generally produce films with excellent optical, e.g. high transparency [8], and electrical, e.g. n-type conductivity [9-11] properties. These materials also exhibit long term environmental stability [12] and bio-compatibility [13,14]. Thus, there exists a body of work on the deposition and properties of thin films of ZnO, AZO and the related materials IGZO (indium- gallium ZnO), IZO (ZnO:In) and ZnO:Ga, on plastic substrates such as as polyethylene terephthalate (PET) [2,5,15-18], polyethylene naphtalate (PEN) [4], polycarbonate (PC) [19], polymethyl methacrylate (PMMA or Perspex) [20], polymide (PI) [3,21] polyester [22] and cyclo-olefin polymer (COP) [23,24].

In the present work, we have used for the first time Zeonor® -a proprietary brand of COP plastics [25]- hereafter referred to as Zeonor, as a substrate for the deposition of ZnO and AZO thin films. Zeonor is the material of choice for many applications in microfluidics [26], bio-diagnostics [27] and biosensors [28], as well as in stringent optics applications such as high density DVDs, liquid crystal displays and plastic optical fibers [25,29]. These and other state-of-the-art devices may variously require the deposition of electrical contacts and/or high-quality optical coatings that could potentially be achieved with ZnO and AZO thin films. Zeonor has unique features compared to other plastic materials [25]; notably, its water absorption of less

than 0.01% is significantly smaller than that of PC (0.2%), PMMA (0.3%) and PET (0.01 to 1.5%) [23,25,30]. Thus, outgassing and water absorption effects in a vacuum environment are minimized, enabling the direct deposition of materials on Zeonor without the need for buffer or barrier layers.

Because the Zeonor glass transition temperature is close to 100 ^{o}C [25], the deposition of good-quality thin films on Zeonor substrate needs to be carried out at or near room temperature. Pulsed laser deposition (PLD) appears a highly suitable and versatile preparation technique to meet this demanding challenge. Indeed, several works have reported the production of high-quality crystalline ZnO/AZO films on amorphous substrates using PLD at room/low temperatures, e.g. [31,32]. PLD at room temperature (RT) is, thus, the growth technique that we use in the present work.

We now recall briefly aspects of ZnO thin film formation relevant to the motivation for the present work. PLD growth of thin-film ZnO is typically carried out in an ambient oxygen pressure, the value of which largely determines the prevalent growth mode, eg. layer-by-layer. In the 1 – 100 mTorr (~ 0.1 –10 Pa) range continuous thin film growth occurs, while upward of 100's mTorr (> 50 Pa) –so-called high-pressure PLD-, film nanostructuring [33] is generally observed with concomitant changes in the microstructure and optoelectronic properties. Such pressure-dependent studies were carried out by Zhu et al. [34] and Gondoni et al. [35,36] on the PLD of ZnO and AZO on glass and sapphire substrates, respectively. During film growth (at a given ambient pressure), the polar ZnO material will undergo significant lattice re-organisation due to defects formation and defects/atomic diffusion, formation of a depletion layer, crystal grain formation and densification. These effects will be reflected in the variations of the film properties with film thickness. For example, Zhu et al. [37] studied the change of the

crystallinity, microstructure and surface morphology of ZnO thin films of various thicknesses prepared by PLD on glass; while Guillen and Herrero [38] conducted a similar study for AZO films of various thicknesses deposited on glass at room temperature by DC sputtering. Finally, all growth parameters being equal, comparison of the properties of ZnO and AZO films will tell the specific effects of doping by aluminium substitution on the zinc lattice sites [10].

Based on these considerations, the aims of our work were to

(1) Use PLD to grow reproducible, high-quality ZnO and AZO thin films on flexible Zeonor plastic substrates at room temperature, and

(2) Reveal the dependency of the growth rates, the microstructure and the surface, structural, optical and electrical properties of ZnO and AZO thin films of different thicknesses on the oxygen ambient pressure. The pressure range explored should correspond with observable changes in the film properties as it is in the range where nanostructuring should occur.

In the rest of the paper, we provide the necessary experimental details. We then present and discuss the results on thin film properties and associated deposition ambient/oxygen pressure and film thickness trends. Finally, we propose applications suitable for the range of film properties obtained in the work.

2. Experimental details

All the films were grown in a standard pulsed laser deposition (PLD) apparatus equipped with a high-power, Q-switched, frequency-quadrupled, Nd:YAG laser [32]. The wavelength output, repetition rate, pulse width and energy of the laser were 266 nm, 10 Hz, 6 ns and 150 mJ, respectively. The average laser fluence on the target was 2.0 J/cm^2. The target-substrate distance was kept constant at 5 cm with the ZnO target being a 99.999% pure sintered ceramic disk of

2.54 cm diameter. The aluminum-doped ZnO (AZO) target was identical in all respects for a 2 wt% Al_2O_3 component equivalent to 3 at% Al. Sheets of 1.2 mm thick 1060R Zeonor [25] cut into 1 cm × 2 cm rectangles were used as substrate. A gentle clean of the bare substrate surfaces with isopropyl alcohol was applied and then dried with nitrogen gas. The Zeonor substrates were mounted and kept at the deposition chamber base pressure of 3×10^{-5} mTorr (3.9×10^{-6} Pa) for about an hour prior to deposition. Growths were carried out in ambient oxygen (deposition) pressures of 75 mTorr (10 Pa), 150 mTorr (20 Pa) and 300 mTorr (30 Pa). From previous literature, see ref. [33] and references therein, in this relatively wide range of deposition pressures, the film growth should span over the transition from 2D layer-by-layer to 3D nanostructuring modes. All the growths were carried out at room temperature and all the samples characterised as-grown, without post-growth high temperature anneal. The details of the growth parameters of the samples produced in this work are given in Table 1.

Film thickness was measured using a Dektak profilometer (D150 Veeco). Surface morphology was studied by atomic force microscopy (AFM) (Dimension 3100 controlled by a nanoscope IIIa controller, digital instruments) in tapping mode. The AFM images were acquired by scanning areas of dimensions 5 μm × 5 μm with a fixed resolution of 512 pixels × 512 pixels. The AFM measurements were repeated several times at three randomly chosen locations of every sample with no remarkable differences found between these locations. The water contact angle (WCA) was measured with the help of a computer-controlled WCA commercial instrument (FTA200 USA) implementing the sessile drop technique. In all the WCA experiments, high-purity HPLC grade water was used and released at a flow rate of 1.5 μL/s from a needle tip 2 mm above the film surface. The quoted WCA values are the average of typically ten measurements on different locations over the surface of the sample and the error

bars represent the corresponding standard deviations. Structural characteristics were investigated by x-ray diffraction using 2θ-ω (Bruker AXS D8) and pole figure (Jordan Valley BEDE-D1) scans, respectively. Optical transmittance spectra were measured using a double-beam UV-vis spectrophotometer (Varian CARRY 50 scan), while low-temperature photoluminescence spectra were recorded with a 1 m focal length monochromator (SPEX 1704) following 325 nm He-Cd laser excitation. Electrical properties were measured with a commercial 4-point probe/Hall effect apparatus (Accent HL5500). The experimental uncertainties or statistical errors associated with all these measurements are recorded, where possible, as error bars on the relevant tables and graphs shown in Section 3.

3. **Results and Analyses**

3.1 **Thickness measurements and growth rate studies**

From Table 1, we see that the range of film thicknesses considered in this work is 74 – 422 nm. Thus, all the films are optically thin and quantum confinement effects are not expected to play any role in the physics underlying their properties. Fig.1 shows the variations of the ZnO and AZO films thickness with the number of laser shots for the three oxygen deposition pressures of 75, 150 and 300 mTorr. For all the samples and growth conditions used, film thickness closely fits a linear function of the number of laser shots (R ~ 1 for the six graphs of Fig.1). From the laser repetition rate of 10 Hz and the slope of each plot, the growth rates are obtained with minimum and maximum values of 0.13 nm/s and 0.22 nm/s respectively. From the inset of Fig.1, where the growth rates are plotted as a function of deposition pressure, we see that the ZnO and AZO film growth rates increase linearly with increasing oxygen deposition pressure at the rates of 2.2×10^{-3} nm/s/10 mTorr and 4.2×10^{-3} nm/s/10 mTorr, respectively. The growth

rates have equalized at 300 mTorr oxygen pressure while the AZO growth rate is about 25% lower than that of ZnO for the lower pressures. From these observations showing linear dependences, we can conclude that similar growth mechanisms leading to optically thin ZnO and AZO films prevail in the range of experimental parameters –notably the 75 – 300 mTorr pressure range- used. Thus, thin film properties of ZnO and AZO can be reproduced when grown on Zeonor substrates by PLD.

3.2 Surface morphology studies

Fig. 2 shows AFM images of the surface of the thickest ZnO (Z3 and Z9) and AZO (A3 and A9) samples as typical examples. The insets of Fig. 2 show that the ZnO and AZO films present similar microstructures, for the two growth pressures of 75 and 300 mTorr, in the form of nanostructured, pea-shaped, grains with typical lateral sizes in the range 50 – 200 nm. Similar nanostructured ZnO deposits have been observed in comparable PLD experiments by many authors [39-42] and also in the laser ablation of silicon [43]. The underlying physical mechanisms have been explained for ZnO in the works of Okada and Kawashima [39] and Hartanto et al. [40]. In short, ZnO nano-clusters of various sizes are initially condensed in the expanding ablation plume and transported to and captured on the substrate. If the substrate is cold and amorphous, as is the case in our work, the nanoparticles have very limited surface diffusion and crystal growth is minimal. The next ablation plume will then build up another patchy layer of similarly shaped nanoparticles and so on. In the case of a high-temperature (and possibly crystalline) substrate, the initial nanoclusters will diffuse rapidly forming a wetting nucleation layer onto which crystalline ZnO nanorods can subsequently grow in a 3D growth mode [42,44]. Relevant to the present work are the fundamental aspects of the synthesis of

silicon nanoclusters by conventional PLD discussed by Marine et al. [43] and the work by Jensen [45] on the growth of nanostructures by cluster deposition. From our previous observation, we can conclude that, all other conditions being equal, the transition to 2D film growth on Zeonor substrate will occur at oxygen pressures lower than 75 mTorr. Overall, the AFM observations and their analyses are consistent with the conclusion, drawn at the end of the previous section, of a similar growth mechanism in the investigated pressure range. On the micrometric length scale (main parts of Fig. 2), no particular organization of the nanostructures can be distinguished and they appear randomly distributed over the observed surface area. On the even larger scale of several tens of microns (not shown here) all the films surfaces were found to be identically smooth, devoid of cracks, fracture lines or delaminations.

We have estimated the values of the average nanostructure lateral grain size and root mean square (rms) roughness R_q for every sample with the help of imaging processing software (WSXM). The results are plotted in Fig. 3. The AFM grain sizes typically range from 75 nm (ZnO) - 90 nm (AZO) for the thinner films to values of 180 nm (ZnO) – 140 nm (AZO) for the thicker films. They are also seen to increase in almost linear fashion with increasing film thickness. The grain size data for the ZnO films show a weak dependency on the oxygen pressure with a pattern of lower pressures producing larger nanostructure grain sizes in films of roughly equal thickness being discernable. Whereas the AZO grain size values appear almost insensitive to the oxygen pressure within the 75 – 300 mTorr range. The ZnO films show a wider dispersion of grain sizes with varying ambient pressure and, on the whole, nanostructure grain sizes are larger by a few 10's of nm for the ZnO films at equal pressure compared with AZO films. Overall the data of Fig. 3 show that the ZnO film morphology results from interplay between ambient pressure and film thickness effects. According to the growth model presented

earlier, for thicker films, the ZnO nanoparticles deposited at a later stage will be captured by a nanostructured ZnO film allowing for better nanocrystal growth leading to larger grains at the lower pressure of 75 mTorr. For AZO, the role of the aluminium dopant in the film growth and lattice reconstruction seems significant to the extent that it appears to shadow the role of the oxygen pressure in the range used. Our experimental observations on grain sizes are generally comparable with previous works on ZnO and AZO nanostructured films deposited on COP and other plastic substrates, e.g. [15,16,24]. The RT PLD work of Gondoni et al. [35,36], in particular, showing that AZO growth on glass becomes granular for oxygen pressures greater than 10 Pa (77 mTorr) supports our findings and the basic model of nanocluster plume formation.

The rms (R_q) surface roughness of the films are represented on the right vertical axes of Fig.3 with different scales for ZnO and AZO. Overall, the trends are similar for the ZnO and AZO films and follow the linear behaviour observed for the nanostructure grain size. The thinner films have R_q values of 1-2 nm, while for the thicker films this is in the range 4-8 nm with the bare Zeonor 1060R surface measured at 0.5 nm [28]. Therefore, all the films are optically smooth for near-normal incidence illumination. Overall, the surface rms roughness increases close to linearly with oxygen pressure for both the ZnO and AZO films. AZO films of comparable thickness have very similar surface roughness, irrespective of the oxygen pressure, while for ZnO films they are more dispersed. Overall, the ZnO films appear to be rougher by several nm's compared with the AZO films in the pressure range used in the work. This is consistent with our observations on grain size just above. The rms surface roughness values of typically a few nanometers reported here compare favourably with those reported in the quoted previous works [15,16,24,34,38]. Authors have pointed out the importance of a smooth surface

for device reliable performance and enhanced lifetime. For example, Han et al. [18] have successfully fabricated AZO TFT's on PET substrates quoting a rms roughness of 1.36 nm, while Connolly et al. have reported the successful deposition of ZnO films on Perspex flexible substrates with a rms roughness of 2.2 nm for use as electrodes in a biofuel cell [20]. The typical roughness of ~ 2 nm for the ZnO and AZO thinner films produced here would thus seem advantageous for similar devices fabricated on flexible Zeonor substrates.

3.3 Water contact angle (WCA) measurements

The wettability of the nanostructured ZnO and AZO thin films was assessed from the variation of the water contact angle (WCA) value with film thickness as shown in Fig. 4. The size of some of the error bars in this figure reflects the large variations of several degrees which were occasionally found between successive measurements on the same sample. This is compatible with the high sensitivity of the ZnO surface wettability on both exposure to near ultraviolet radiation [46] and chemical contamination [47]. A WCA of 92.0° has been measured for the bare 1060 R Zeonor surface, which is therefore hydrophobic [25,26,28]. Overall, it is seen that the main effect of ZnO and AZO thin film deposition is to increase the hydrophobicity of the Zeonor surface. However, the ZnO and AZO films show marked differences in this regard when considering the thickness and pressure dependences. For the ZnO films, it is seen that the WCA increases with thickness at all pressures, but the rate of increase is inversely proportional to the oxygen pressure. Indeed, for a 75 mTorr deposition pressure, the ZnO WCA is seen to increase to a maximum value of about 110° for the 340 nm film, while it increases only to about 95° for the 422 nm film deposited at 300 mTorr. For the AZO films, the general trend is a slight decrease of the WCA as a function of film thickness, from about 94° to slightly less than 92° and almost

within the error bar, while there appears to be little sensitivity of this decrease on the ambient oxygen pressure. The WCA data of Fig.4 can be correlated with the microstructure data of Fig.3. The larger WCA values for the thicker ZnO films correspond with the larger nanostructure sizes and rms surface roughnesses observed at the 75 mTorr pressure while the aforementioned lack of sensitivity of the rms roughness on the film thickness and deposition pressure is also seen in the WCA trends for AZO. This is indicative of a lower surface energy for the rougher surfaces which, thus, exhibit larger contact angles [48]. The present results confirm the work of Subedi et al. [49] showing a WCA greater for ZnO than for AZO films and that of Sun et al. [46] reporting the dependence of the ZnO surface wettability on its surface morphology.

3.4 Structural properties

Fig.5 shows the out-of-plane 2θ-ω xrd angular scans measured in the $2\theta \approx 32^{o}$-38° range for all the ZnO and AZO samples. All these scans showed a single dominant (002) peak with a weak (101) peak appearing for some of the AZO samples. More extended angular scans also include the broad Zeonor substrate peak at $2\theta \approx 16^{o}$ as shown in the inset (Z3 sample). These data show that all the ZnO and AZO thin films deposited on Zeonor substrates by PLD have the wurtzite crystalline structure and are highly textured with *c*-axis orientation, i.e. the hexagonal (002) plane (basal plane) lies parallel to the plane of the substrate. The AZO material has a more polycrystalline structure in the thicker films with some grains showing the (101) plane (facet) lying parallel to the substrate plane. It is observed from Fig.5 that the (002) peaks are more intense and narrower for ZnO than AZO films of comparable thickness. In order to establish the effect of oxygen pressure on crystalline quality, the integrated intensity of the (002) peaks was plotted as a function of film thickness for the various growth pressures used in this work. The plots are shown in the insets of Fig.5 with added linear trend lines: The effect of pressure on

crystalline quality can be assessed by reading the graph along a vertical line of constant film thickness. It is seen that for both the ZnO and AZO films crystalline quality is significantly better at the oxygen pressure of 75 mTorr. While for the AZO films crystalline quality appears less sensitive to oxygen pressure being almost pressure-independent at 150 and 300 mTorr. This is also true for both the ZnO and AZO films of thickness less than or equal to 100 nm. From Fig.3 (AFM data), we note that for these films the lateral grain size is of the same order as the thickness. Thus, the films crystalline structure is likely to be initially dominated by the unfavourable interface between the cold amorphous Zeonor surface and the ZnO and AZO nanocrystals. Further film growth atop ZnO or AZO material will then favour better lattice reconstruction minimising surface energy by favouring *c*-axis orientation. This accounts for the general increase of crystalline quality with thickness seen in the inset of Fig.5. For AZO, the point defects introduced by the aluminium dopant will also play a role in this regard as the thickness increases (see pole figure data below). The complete set of data of Fig.5 points to the enhanced crystalline quality of the ZnO material compared to the AZO material in films grown on thin amorphous Zeonor plastic substrates at room temperature.

The 2θ angular position and full width at half maximum (FWHM) of the (002) peak as well as the *c*-axis length are given in Table 1 for all the samples. For reference, we have also measured with the same apparatus, shown in Fig.5 with scale downed intensity, a 2θ value of 34.45º for a 0.5 mm thick *c*-axis oriented ZnO single-crystal wafer (Tokyo Denpa). We use the (002) peak FWHM values and 2θ angular positions to estimate the samples crystallite size and residual stress, respectively, The average crystallite size D can be calculated [50] using Scherrer equation $D = \frac{0.9\lambda}{\beta_{hkl}\cos\theta_B}$, where λ = 0.15425 nm is the wavelength of the Cu K_α line, θ_B is the

Bragg angle and $\beta_{hkl} = \sqrt{\left(\beta_{hkl}^{meas}\right)^2 - \left(\beta_{hkl}^{instr}\right)^2}$ is the 2θ FWHM of the ZnO (002) peak after removal of the instrumental broadening assuming Gaussian line profiles. The instrumental contribution is estimated from the value of the 2θ FWHM for the (002) peak of the single-crystalline ZnO wafer measured at 0.167°, thus, assuming an essentially infinite "crystallite" size for this sample. The corresponding graphs are shown in Fig.6 from which we see that crystallite sizes are in the ranges 20 – 25 nm and 12 – 18 nm for the ZnO and AZO films, respectively. Overall, the larger D values observed for the ZnO samples are further evidence of the better crystalline quality of the ZnO compared to the AZO material. The small variations of D observed with oxygen pressure and sample thickness in the measured ranges appear not significant being roughly within or just outside of the error bars (relative error of about 5% on D for the strongest peak of Fig.5). The present as-grown crystallite size values are similar to literature values obtained in comparable experimental conditions, with additional temperature anneals applied by some of the authors. Zhu et al. [37] report values of 15 and 25 nm for 50 and 225 nm thick ZnO films, respectively, grown at an oxygen pressure of 12 Pa (~100 mTorr) on glass substrates heated at 350 °C. In the present case of Zeonor substrates, the increase in crystallite size with ZnO film thickness seen in [37] is not retrieved, while the same increase with oxygen pressure reported in [34] is broadly confirmed here. A mean crystallite size of about 23 nm for ~250 nm thick AZO films grown on PET substrate at RT and oxygen pressure of 0.4 Pa (3 mTorr) is reported in refs [6,38], while this is around 10 nm for 500 nm thick AZO films grown on glass substrates at RT and 10 Pa (75 mTorr) oxygen pressure [36]. The small increase in crystallite size with film thickness reported in [6,38] is also observed in the present work, while the general trend of a larger AZO crystallite size with decreasing pressure shown in [35,36] is generally followed here for AZO films on Zeonor substrates.

The residual stress in the ZnO film plane σ is proportional to the strain along the c-axis in the biaxial strain model and can be estimated from equation (1)

$$\sigma = -4.54 \times 10^{11} \frac{(c - c_0)}{c_0} \text{ Nm}^{-2} \qquad (1)$$

where c and c_0 are the c-axes length of the strained and relaxed ZnO crystal, respectively [51]. The c-axis length and stress values of all the samples are shown in Table 1 and Fig.7, respectively. As the films are grown at RT, thermal stress components are neglected. The experimental value of the c-axis length for the ZnO single-crystal wafer is taken as the c_0 value of 0.5207_2 nm. This is obtained from values of $2\theta_{(002)} = 34.45_1^{\circ}$ and $\lambda = 0.15425$ nm and matches accurately the ZnO c-axis length of 0.520690 nm (JCPDS card number 36-1451) when rounded off to the third decimal place. This shows that the film stress values estimated from the measured change in the length of the c-axis are significant and reliable. A pointing error of ± 0.005° on the Bragg angle value yields an absolute error of ± 0.0002 nm on the c-axis length. The corresponding relative errors on the c-axis strain/film stress amount to about 5% and 15% for c-values of 0.5244 nm and 0.5220 nm, respectively. From equation (1), it is seen that this relative error gets larger as the c-axis length gets closer to c_0, while a negative σ value indicates a film in a compressive state of stress with its c-axis length larger than c_0. Fig.7 shows that the ZnO and AZO films are in a compressive state of stress with σ values of –(2–3) GPa and -0.5 GPa, respectively. The AZO films follow a similar trend. It is also seen that the stress has changed from compressive to tensile in the case of the AZO films grown at 300 mTorr (see below the discussion of pole figures). For all the films, except the latter, the stress values decrease linearly with film thickness at a given pressure indicating a relief of in-plane stress for the thicker films. Overall, the ZnO films grown at the lower oxygen pressure of 75 mTorr have less in-plane compressive stress than those grown at the higher pressures of 150 and 300 mTorr. These

observations are consistent with our previous conclusions on both crystalline quality and growth mechanisms. The compressive stress values for the ZnO films on Zeonor substrates are comparable with those (~ -2 GPa) in the work of Maniv et al. [51] in which RT glass substrates were used, but differ from those of Zhu et al. [37] and Novotny et al. [52] in which tensile stress values of ~ 0.3 and 0.9 GPa were found for ZnO deposited on glass. Deposition temperatures of ~ 350 ºC were used in these last two works as well as a 750 ºC oxygen anneal in [52]. Thus, deposition and processing temperatures significantly larger than RT can lead to different mechanical states for a ZnO film. For AZO films, the compressive stress diminishes compared to ZnO due to the smaller ionic radius of Al^{3+} substituting on the Zn^{2+} sites. The σ or *c*–axis length values obtained here for AZO on Zeonor substrates are similar with comparable works quoted previously [6,10,36].

In order to investigate further the effects of deposition pressure on the texture and *c*-axis orientation of our ZnO and AZO thin films, we have measured the corresponding (002) pole figures for the selected samples Z3, Z9, A3 and A9 (same as in Fig. 2). The results are shown in Fig.8. The ZnO pole figures show high circular symmetry with narrow widths of 20° (75 mTorr) and 22° (300 mTorr) indicating a uniform alignment of the *c*-axis with small angular distribution about the substrate surface normal. The narrower and more intense pattern for sample Z3 suggests that the 75 mTorr deposition pressure creates better textured ZnO films. Kim et al. [24] have reported similar observations for Al and Ga doped ZnO films grown by RF sputtering. The AZO films appear to also follow this trend although the pole figures are much broader with widths of 34° (75 mTorr) and 54° (300 mTorr) indicating large variations of the *c*-axis orientation about the surface normal in the doped films. For sample A9 (AZO, 300 mTorr) the pole figure intensity maximum is split and off-centered indicating an overall tilt of the *c*-axis by

about 5° with respect to the normal to the substrate surface. It has been shown that the state of stress in this sample was uniquely tensile as opposed to compressive for all the other ZnO and AZO films. From the pole figure study, we can conclude that both Al-doping and deposition pressure have noticeable effects on the *c*-axis orientation of thin ZnO films deposited on Zeonor substrates indicating the sensitivity of the growth mode to these two parameters. We note here that Takayanagi et al. have shown recently that tilted *c*-axis ZnO layered structures can be used as ultrasonic transducers [53] and our work thus shows an experimental route for the fabrication of such structures.

3.5 Optical properties

The effect of deposition pressure on the optical properties/quality of the ZnO and AZO films of different thickness has been studied using UV-vis absorption spectroscopy and low temperature photoluminescence spectroscopy.

3.5.1 Transmission studies

The transmission spectra of the ZnO and AZO samples, referenced to the bare Zeonor substrate (visible transmission of 90%), are shown in Fig.9. All the spectra show the absorption onset behavior characteristic of the direct band gap of ZnO consisting of almost complete transparency in the visible region followed by a sharp cut off in the near ultraviolet, around 370 nm for ZnO and 350 nm for AZO, and almost complete absorption at the shorter wavelengths. All the samples are characterised by a visible transparency of at least 85-90% and this can even be greater than 95% for some samples. The enhancement effect of multiple interferences due to

multiple reflections at the air/ZnO-AZO/Zeonor/air interfaces is clearly present and indicative of the high sharpness of these interfaces.

It has been shown by several authors [52,54] that the commonly used method for determining the "optical band gap" E_g^{opt} based on an extrapolation to $\alpha = 0$ of the linear part of the α^2 vs $h\nu$ graph, where α and $h\nu$ are the absorption coefficient and photon energy respectively, systematically underestimates the value of E_g^{opt}, due to the presence of excitonic and other effects in ZnO which the Tauc model does not take into account. In addition, this method can lead to significant absolute errors for thick films (100 nm or greater) as the transmission values at the higher photon energies are then much less than a few percents and contain significant noise. We have thus evaluated the absorption edge energy from the transmission spectra using the following procedure to ensure a consistent approach allowing discussion of systematic trends. In the vicinity of the absorption edge, the ZnO and AZO layers are heavily absorbing and the transmittance assumes a simple exponential form from which the value of the absorption coefficients can be estimated with the knowledge of the layer thickness [10,55]. Typical results, showing α in cm^{-1} as a function of $h\nu$ in eV on a semi-log plot, are shown in the insets of Fig. 9 (for Z3 and A3 samples). It is seen (for ZnO) that the value of α is around 1.3×10^5 cm^{-1} near the edge without any distinct excitonic structure as would be expected in un-annealed samples [56]. For all the other samples, we found values of α in the $(0.9 - 2.0) \times 10^5$ cm^{-1} range near the absorption edge which, thus, fall in the expected domain [54]. The value of the absorption edge can be estimated from semi-log plots of α vs $h\nu$ [57,58]. We have applied the graphical method depicted in the insets of Fig.9 systematically to all the ZnO and AZO samples data to estimate their fundamental absorption edge energy (with ±1% relative

error). In the following, we treat these absorption edge values as our best estimation of the optical band gap values although we cannot properly take into account the 60 meV exciton binding energy and thus we still slightly underestimate the band gap. The results are shown in Fig.10 from which it is seen that the absorption edge energy of all the ZnO films is almost constant near an average value of 3.34 eV. This is just slightly less than the 3.37 eV band gap energy of bulk ZnO at room temperature [54] and thus confirms the validity of our method of estimation of the band gap energy. The variations of the ZnO optical band gap energy as a function of thickness and deposition pressure are observed to be mild. This behaviour of the band gap energy is compatible with the relatively small variations of the stress and grain size values on deposition pressure and thickness that we have discussed in the previous sections. In the comparable PLD works of Zhu et al. [34,37] and Novotný et al. [52], "Tauc band-gap" energies of 3.25 eV and 3.28 eV for ZnO films of similar thickness are reported and discussed by the authors. For the AZO films a more dispersed pattern is observed on Fig.10 with values varying between 3.48 eV and 3.60 eV about a mean of 3.54 eV, larger than ZnO, as expected, as a result of the increased n-type dopant concentration. As the electron carrier densities measured (see Section 3.6 below) are typically much lower than the ZnO critical density of ~10^{19} cm^{-3}, the observed band gap widening for AZO can be largely attributed to the Burstein-Moss shift [10,11,59]. Use of the Tauc plot method to determine E_g^{opt} in AZO (2 wt% Al_2O_3) gave values of 3.68 eV for RT deposition on PET substrates [6], 3.4 eV for RT deposition on glass substrates [35] and 3.45 eV for 400 ºC deposition on fused quartz substrates [10]. Our data lies within this spread of literature values. From Fig.10, the band gap energies for the 300 mTorr AZO films are seen consistently lower than for AZO films grown at the lower pressures and this can be related to our previous observation of a significant compressive to tensile change in the in-plane stress

for 300 mTorr AZO films. This behavior is similar to that reported by Mohanty et al. [60]. A trend whereby the AZO optical band gap slightly decreases in a linear fashion with film thickness is just discernable above the error margin in Fig.10. Again, this could be related to the corresponding grain size/stress behaviours discussed above.

3.5.2 Photoluminescence studies

Fig.11 shows the low temperature (13 K) photoluminescence spectra of the thickest (20,000 laser shots) of our ZnO and AZO thin films (samples Z3, Z6, Z9 and A3, A6, A9) for the three pressures of 75 mTorr, 150 mTorr and 300 mTorr used in this work. The spectra of the ZnO films show the characteristic near band edge (NBE) emission in the near UV emission and the deep-level emissions (DLE) in the visible spectrum composed of the yellow (2.2 eV) and orange/red (1.9 eV) bands. The NBE band is due to excitonic recombinations while the yellow and orange/red DLE emissions are defect bands usually attributed to oxygen interstitials [61-63]. The NBE bands are significantly more intense than the defect bands at any deposition pressure, testifying to the good optical quality of the ZnO material in the films. It is seen that the NBE peak emission wavelength shifts from 392 nm to 385 nm when the oxygen pressure increases from 75 mTorr to 300 mTorr. As this 7 nm wavelength shift is small, it cannot be conclusively correlated with the equally small differences in energy gap seen in Fig.10 for these samples.

For the AZO films, a strong NBE band is observed for all the oxygen pressures with a complete quenching of the deep level emissions. This effect is known and several reasons have been invoked in the literature to explain the absence of DLE in AZO films, see e.g. [64], though, to the best of our knowledge no consensus has yet been reached. We put forward one plausible explanation for the quenching of the DLE band in AZO. Native defects in ZnO, such as the oxygen interstitials responsible for the DLE, have higher formation energy in AZO than in ZnO

due to the presence of aluminium which has a very strong chemical affinity for oxygen. Thus, oxygen displacement from its normal binding site is energetically less favorable in AZO compared to undoped ZnO. The concentration of oxygen interstitials may then be reduced when Al is incorporated during growth and hence no DLE is observed in AZO films. The AZO NBE peak emission wavelengths have blue-shifted to around 380 nm which is consistent with our previous observation of an increased band gap energy for AZO. Finally, we note that the NBE emission intensity is significantly reduced for the 300 mTorr AZO sample indicating that the optical quality of the material is highly sensitive to the oxygen deposition, in accord with the markedly different structural and mechanical properties already noted for this sample.

3.6 Electrical properties

Fig.12 shows the electrical properties of the ZnO and AZO samples in the form of the variations of Hall mobility and carrier concentration with film thickness for the various deposition pressures while the resistivity values are given in Table 1. It is worthwhile recalling here that all the measurements were carried out on the as-grown films without any thermal annealing or carrier activation treatments. For the ZnO films deposited at 75 mTorr, high resistivity values of 5×10^{5} Ω cm (85 nm film), 2×10^{4} Ω cm (169 nm film) and 4×10^{5} Ω cm (340 nm film) and carrier concentrations $\leq 10^{9}$ cm^{-3} were typically obtained. Hall effect measurements on these highly resistive samples turned out to be too noisy and unreliable. The 75 mTorr ZnO samples typically exhibit semi-insulating behavior. For the ZnO samples grown at the higher pressures of 150 mTorr and 300 mTorr, resistivity values tend to drop by 2-3 orders of magnitude, down to 1.5×10^{2} Ω cm (92 nm thick sample at 150 mTorr), although some remain high, for example 2×10^{4} Ω cm (209 nm thick sample at 300 mTorr). Hall mobility values for

these samples are all around 1 cm^2/V s, whereas n-type carrier concentration values vary between 5×10^{14} cm^{-3} and 5×10^{16} cm^{-3}. Overall, the electrical behavior of the ZnO/Zeonor samples varies significantly from semi-insulating to n-type semiconducting as a function of the oxygen deposition pressure. This pattern for ZnO thin films deposited by PLD under similar oxygen pressure conditions has been observed by many workers; see for example, Grundmann et al. [65].

As expected, the electrical properties of the AZO thin films tend to show an improved conductive behavior compared to ZnO. Notably, the resistivity values have all dropped significantly at all growth pressures and are mostly found in the range 4×10^2 Ω cm - 2×10^3 Ω cm for the lower pressures of 75 mTorr and 150 mTorr and around 9×10^3 Ω cm for the films grown at 300 mTorr. Hall mobility values are significantly increased in AZO compared with ZnO, with the bulk of the values found in the range 4 - 14 cm^2/V-s with n-type carrier concentrations in the range 10^{15} cm^{-3} - 5×10^{16} cm^{-3}. The data of Fig. 12 show that resistivity values tend to increase with both pressure and film thickness. The strong dependence of the resistivity of as-deposited AZO films grown by PLD at RT on glass with oxygen pressure was shown in ref [35], with the resistivity tending to insulator values at pressures of 10 Pa (75 mTorr) and greater. This behaviour is also verified in our work. Lu et al. [10] have also shown that the AZO electrical properties depend critically on the Al concentration with increase in resistivity from 10^{-3} Ω cm to 100 Ω cm when the concentration drops from about 3 at% to 1.5 at%. The AZO Hall mobility, resistivity and carrier density values reported in the present work are generally compatible with those of ref [10]. The 4 - 14 cm^2/V-s Hall mobility values for the AZO films obtained here would be suitable for use in transparent flexible thin film transistor applications [5], for example. For applications requiring transparent conductive oxide (TCO) properties, the AZO resistivity would

be significantly lowered (by a couple of orders of magnitude) and match that of other works on plastic substrates [6,12,15], by (i) carrying out the depositions at oxygen pressures in the 0.1 – 1 Pa (0.75 mTorr- 7.5 mTorr) range and (ii) non-thermal post-processing of the films using laser annealing [66].

4. Conclusions

In this work, we have shown for the first time that ZnO and Al-doped ZnO (AZO) nanocrystalline thin films with high material quality can be reproducibly grown on flexible Zeonor plastic substrates using pulsed laser deposition at room temperature. We have also systematically studied the effects of oxygen in a selected pressure range on the growth rate, surface morphology, hydrophobicity and the structural, optical and electrical properties of films having different thicknesses.

All the films were observed to have the same nanostructured morphology. This was shown to be compatible with existing film growth models based on the capture by the Zeonor substrate of nanoclusters that have condensed in the expanding ablation plume. Highly linear growth rates were obtained showing that ZnO and AZO films with identical properties can be reproducibly deposited using the PLD technique. The deposition of ZnO or AZO films was shown to significantly enhance the hydrophobicity of the Zeonor plastic surface. All the films were nanocrystalline (wurtzite structure) with high texture (*c*-axis orientation) and good crystallinity. Their optical quality was good: All the ZnO and AZO films displayed high visible transparency, greater than 95% in some cases, while their low temperature photoluminescence spectra showed intense near band edge emission. A considerable spread from semi-insulating to n-type conductive was observed in the ZnO and AZO films electrical behavior, with marked

dependences on film thickness and oxygen deposition pressure. The resistivity values of typically around 10^3 Ω cm and Hall mobility values in the range 4 - 14 cm^2/Vs showed that the ZnO and AZO films would be suitable for applications in flexible sensors, transducers and transparent thin film transistors. As Zeonor plastics are used in many healthcare and medical applications, our work has shown convincingly that ZnO and AZO electrodes on Zeonor flexible substrates could be used advantageously in microfluidic, bio-sensing or biofuel-cell energy applications, for example.

ACKNOWLEDGMENTS

Saikumar Inguva acknowledges the award of a postgraduate studentship from “INSPIRE (Integrated Nanoscience Platform for Ireland)”. This work was conducted under the framework of the Irish Government’s Programme for Research in Third Level Institutions Cycle 5, National Development Plan 2007-2013 with the assistance of the European Regional Development Fund. The authors also acknowledge J. Gaughran, J. Ducree, J. Connolly, B. O’Connell, A. A. Cafolla, E. McCarthy, P. J. McNally and C. S. Wong for their help with experiments and helpful discussions during the course of this work.

References

[1] Lee J, Lee P, Lee H B, Hong, Lee I, Yeo J, Lee S S, Kim T S and Lee D 2013 Room-Temperature Nanosoldering of a Very Long Metal Nanowire Network by Conducting-Polymer-Assisted Joining for a Flexible Touch-Panel Application *Adv. Funct. Mater.* **23** 4171-4176.

[2] Chang G J, Lin S Y and Wu J J 2014 Room-temperature chemical integration of ZnO nanoarchitectures on plastic substrates for flexible dye-sensitized solar cells *Nanoscale* **6** 1329-1334.

[3] Park J S, Kim T W, Stryakhilev D, Lee J S, An S G, Pyo Y S, Lee D B, Mo Y G, Jin D U and Chuang H K 2009 Flexible full color organic light-emitting diode display on polyimide

plastic substrate driven by amorphous indium gallium zinc oxide thin-film transistors *Appl. Phys. Lett.* **95** 013503.

[4] Hwang Y H, Seo J S, Yun J M, Park H, Yang S, Park S H K and Bae B S 2013 An 'aqueous route' for the fabrication of low-temperature-processable oxide flexible transparent thin-film transistors on plastic substrates *NPG Asia Mater.* **5** e45.

[5] Nomura K, Ohta H, Takagi A, Kamiya T, Hirano M and Hosono H 2004 Room-temperature fabrication of transparent flexible thin-film transistors using amorphous oxide semiconductors *Nature* **432** 488-492.

[6] Guillen C and Herrero J 2009 Structure, optical and electrical properties of Al:ZnO thin films deposited by DC sputtering at room temperature on glass and plastic substrates *Phys. Status Solidi A* **206** 1531-1536.

[7] Hong Y, He Z, Lennhoff N, Banach D A and Kanicki J 2004 Transparent flexible plastic substrates for organic light-emitting devices *J. Electron. Mater.* **33** 312-320.

[8] Hagendorfer H, Lienau K, Nishiwaki S, Fella C M, Kranz L, Uhl A R, Jaeger D, Luo L, Gretener C, Buecheler S, Romanyuk Y E and Tiwari A N 2014 Highly Transparent and Conductive ZnO: Al Thin Films from a Low Temperature Aqueous Solution Approach *Adv. Mater.* **26** 632-636.

[9] Wang Z L 2007 Novel nanostructures of ZnO for nanoscale photonics, optoelectronics, piezoelectricity, and sensing *Appl.Phys. A:Mater. Sci. Process.* **88** 7-15.

[10] Lu J G, Ye Z Z, Zeng Y J, Zhu L P, Wang L, Yuan J, Zhao B H and Liang Q L 2006 Structural, optical, and electrical properties of (Zn,Al)O films over a wide range of compositions *J. Appl. Phys.* **100** 073714.

[11] Lu J G, Fujita S, Kawaharamura T, Nishinaka H, Kamada Y, Ohshima T, Ye Z Z, Zeng Y J, Zhang Y Z, Zhu L P, He H P and Zhao B H 2007 Carrier concentration dependence of band gap shift in n-type ZnO:Al films *J. Appl. Phys.* **101** 083705.

[12] Zhang D H, Yang T L, Ma J, Wang Q P, Gao R W and Ma H L 2000 Preparation of transparent conducting ZnO:Al films on polymer substrates by r. f. magnetron sputtering *Appl. Surf. Sci.* **158** 43-48.

[13] Liu Y, Zhong M, Shan G, Li Y, Huang B and Yang G 2008 Biocompatible ZnO/Au nanocomposites for ultrasensitive DNA detection using resonance Raman scattering *J. Phys. Chem. B* **112** 6484-6489.

[14] Sadik P W, Pearton S J, Norton D P, Lambers E and Ren F 2007 Functionalizing Zn- and O-terminated ZnO with thiols *J. Appl. Phys.***101** 104514.

[15] Socol G, Socol M, Stefan N, Axente E, Popescu-Pelin G, Craciun D, Duta L, Mihailescu C N, Mihailescu I N, Stanculescu A, Visan D, Sava V, Galca A C, Luculescu C R and Craciun V 2012 Pulsed laser deposition of transparent conductive oxide thin films on flexible substrates *Appl. Surf. Sci.* **260** 42-46.

[16]Sierros K A, Banerjee D A, Morris N J, Cairns D R, Kortidis I and Kiriakidis G 2010 Mechanical properties of ZnO thin films deposited on polyester substrates used in flexible device applications *Thin Solid Films* **519** 325-330.

[17]Yang R Y, Weng M H, Pan C T, Hsiung C M and Huang C C 2011 Low-temperature deposited ZnO thin films on the flexible substrate by cathodic vacuum arc technology *Appl. Surf. Sci.* **257** 7119-7122.

[18](a) Han D, Wang W, Cai J, Wang L, Ren Y, Wang Y and Shengdong Z 2013 Flexible Thin-Film Transistors on Plastic Substrate at Room Temperature *J. Nanosci. Nanotechnol.* **13** 5154-5157 (b) Han D, Zhuofa C, Zhao N, Wang W, Huang F, Zhang S, Zhang X and Wang Y 2014 Flexible aluminum-doped zinc-oxide thin-film transistor fabricated on plastic substrates *Proc. SPIE USA* **8987** 89871L (doi: 10.1117/12.2044554).

[19]Gong L, Lu J and Ye Z 2010 Transparent and conductive Ga-doped ZnO films grown by RF magnetron sputtering on polycarbonate substrates *Sol. Energy Mater. Sol. Cells* **94** 937-941.

[20]Connolly J, Jain A, Pastorella G, Krishnamurthy S, Mosnier J P and Marsili E 2011 Zinc oxide and indium tin oxide thin films for the growth and characterization of Shewanella loihica PV-4 electroactive biofilms *Virulence* **2** 479-482.

[21]Matsumura M and Camata R P 2005 Pulsed laser deposition and photoluminescence measurements of ZnO thin films on flexible polyimide substrates *Thin Solid Films* **476** 317-321.

[22]Fortunato E, Nunes P, Costa D, Brida D, Ferreira I and Martins R 2002 Characterization of aluminium doped zinc oxide thin films deposited on polymeric substrates *Vacuum* **64** 233-236.

[23]Miyake A, Yamada T, Makino H, Yamamoto N and Yamamoto T 2008 Effect of substrate temperature on structural, electrical and optical properties of Ga-doped ZnO films on cyclo olefin polymer substrate by ion plating deposition *Thin Solid Films* **517** 1037-1041.

[24]Kim J P, Bae J S, Hong T E, Won M S, Yoon J H, Lee B S and Lee H J 2010 Optical and electrical properties of ZnO films, codoped with Al and Ga deposited at room temperature by an RF sputtering method *Thin Solid Films* **518** 6179-6183.

[25]Zeon corporation: www.zeon.co.jp (last accessed 6th June 2015).

[26]Laib S and MacCraith B D 2007 Immobilization of biomolecules on cyclo olefin polymer supports *Anal. Chem.* **79** 6264-6270.

[27]Gandhiraman R P, Volcke C, Gubala V, Doyle C, Basabe-Desmonts L, Dotzler C, Toney M F, Iacono M, Nooney R I, Daniels S, James B and Williams D E 2010 High efficiency amine functionalization of cyclo olefin polymer surfaces for biodiagnostics *J. Mater. Chem.* **20** 4116-4127.

[28]Volcke C, Gandhiraman R P, Gubala V, Raj J, Cummins Th, Fonder G, Nooney R I, Mekhalif Z, Herzog G, Daniels S, Arrigan D W M, Cafolla A A and Williams D E 2010 Reactive amine surfaces for biosensor applications, prepared by plasma-enhanced chemical vapour modification of polyolefin materials *Biosens. Bioelectron.* **25** 1875-1880.

[29]Obuchi K, Komatsu M and Minami K 2007 High performance optical materials cyclo olefin polymer ZEONEX *Proc. SPIE USA* **6671** 66711I (doi:10.1117/12.749910).

[30]Yamazaki M 2004 Industrialization and application development of cyclo-olefin polymer *J. Mol. Catal. A:Chem.* **213** 81-87.

[31]Matsubara K, Fons P, Iwata K, Yamada A and Niki S 2002 Room-temperature deposition of Al-doped ZnO films by oxygen radical-assisted pulsed laser deposition *Thin Solid Films* **422** 176-179.

[32]Mosnier J P, O'Haire R J, McGlynn E, Henry M O, McDonnell S J, Boyle M A and McGuigan K G 2009 ZnO films grown by pulsed-laser deposition on soda lime glass substrates for the ultraviolet inactivation of Staphylococcus epidermidis biofilms *Sci. Technol. Adv. Mater.* **10** 045003.

[33]Eason R 2007 *Pulsed Laser Deposition of Thin films: Applications-Led growth of Functional Materials* Ch.12 pp.278-285 (Hoboken, NJ: Wiley).

[34]Zhu B L, Zhao X Z, Xu S, Su F H, Li G H, Wu X G, Wu J, Wu R and Liu J 2008 Oxygen pressure dependences of structure and properties of ZnO films deposited on amorphous glass substrates by pulsed laser deposition *Jpn. J. Appl. Phys.* **47** 2225-2229.

[35]Gondoni P, Ghidelli M, Di Fonzo F, Carminati M, Russo V, Bassi A L and Casari C S 2012 Structure-dependent optical and electrical transport properties of nanostructured Al-doped ZnO *Nanotechnology* **23** 365706.

[36]Gondoni P, Ghidelli M, Di Fonzo F, Russo V, Bruno P, Marti-Rujas J, Bottani C E, Bassi A L and Casari C S 2012 Structural and functional properties of Al:ZnO thin films grown by Pulsed Laser Deposition at room temperature *Thin Solid Films* **520** 4707-4711.

[37]Zhu B L, Sun X H, Guo S S, Zhao X Z, Wu J, Wu R and Liu J 2006 Effect of thickness on the structure and properties of ZnO thin films prepared by pulsed laser deposition *Jpn. J. Appl. Phys.* **45** 7860-7865.

[38]Guillen C and Herrero J 2010 Optical, electrical and structural characteristics of Al:ZnO thin films with various thicknesses deposited by DC sputtering at room temperature and annealed in air or vacuum *Vacuum* **84** 924-929.

[39]Okada T and Kawashima K 2004 Synthesis of a variety of ZnO nanostructured crystals by nanoparticle-assisted pulsed-laser deposition *Proc. SPIE Japan* **5662** 420 (doi:10.1117/12.596394).

[40]Hartanto A B, Ning X, Nakata Y and Okada T 2004 Growth mechanism of ZnO nanorods from nanoparticles formed in a laser ablation plume *Appl. Phys. A* **78** 299-301.

[41]O'Haire R, McGlynn E, Henry M O and Mosnier J P 2007 ZnO nanostructured thin films grown by pulsed laser deposition in mixed O_2/Ar background gas *Superlat. Microstruct.* **42** 468-472.

[42]Okada T, Agung B H and Nakata Y 2004 ZnO nano-rods synthesized by nano-particle-assisted pulsed-laser deposition *Appl. Phys. A* **79** 1417-1419.

[43]Marine W, Patrone L, Luk'yanchuk B and Sentis M 2000 Strategy of nanocluster and nanostructure synthesis by conventional pulsed laser ablation *Appl. Surf. Sci.***154** 345-352.

[44]Inguva S, Marka S K, Vijayaraghavan R K, McGlynn E, Srikanth V V S S and Mosnier J P 2015 Crystalline ZnO/Amorphous ZnO Core/Shell Nanorods: Self-Organized Growth, Structure, and Novel Luminescence *J. Phys. Chem. C* **119** 4848-4855.

[45]Jensen P 1999 Growth of nanostructures by cluster deposition: Experiments and simple models *Rev. Mod. Phys.* **71** 1695-1735.

[46]Sun M, Du Y, Hao W, Xu H, Yu Y and Wang T 2009 Fabrication and Wettability of ZnO Nanorod Array *J. Mater. Sci. Technol.* **25** 53-57.

[47]Guo M, Diao P and Cai S 2007 Highly hydrophilic and superhydrophobic ZnO nanorod array films *Thin Solid Films* **515** 7162–7166.

[48]De Gennes P G 1985 Wetting -Statics and Dynamics *Rev. Mod. Phys.* **57** 827-863.

[49]Subedi D P, Madhup D K, Sharma A, Joshi U M and Huczko A 2011 Study of the Wettability of ZnO Nanofilms *Int. Nano Lett.* **1** 117-122.

[50]Mote V D, Purushotham Y and Dole B N 2012 Williamson-Hall analysis in estimation of lattice strain in nanometer-sized ZnO particles *Journal of Theoretical and Applied Physics* **6** 1-8.

[51]Maniv S, Westwood W D and Colombini E 1982 Pressure and angle of incidence effects in reactive planar magnetron sputtered ZnO layers *J. Vac. Sci. Technol.* **20** 162-170.

[52]Novotny M, Cizek J, Kuzel R, Bulir J, Lancok J, Connolly J, McCarthy E, Krishnamurthy S, Mosnier J P, Anwand W and Brauer G 2012 Structural characterization of ZnO thin films grown on various substrates by pulsed laser deposition *J. Phys.D: Appl. Phys.* **45** 225101.

[53]Takayanagi S, Yanagitani T and Matsukawa M 2012 Wideband Multimode Transducer Consisting of c-Axis Tilted ZnO/c-Axis Normal ZnO Multilayer *Jpn. J. Appl. Phys.* **51** 07GC08.

[54]Klingshirn C F, Meyer B K, Wagg A, Hoffman A and Geurts J 2010 *Zinc Oxide-From Fundamental Properties Towards Novel Applications* **120** Ch. 6 pp.149-150 (Berlin: Springer).

[55]Heavens O S 1991*Optical Properties of Thin Solid Films* Ch. 4 pp.77 (New York: Dover).

[56]Muth J F, Kolbas R M, Sharma A K, Oktyabrsky S and Narayan J 1999 Excitonic structure and absorption coefficient measurements of ZnO single crystal epitaxial films deposited by pulsed laser deposition *J. Appl. Phys.* **85** 7884-7887.

[57]Yu P Y and Cardona M 2010 *Fundamentals of semiconductors: Physics and Materials Properties* Ch. 6 pp. 270 (Berlin: Springer).

[58]Johnson E J and Fan H Y 1965 Impurity and Exciton Effects on the Infrared Absorption Edges of III-V Compounds *Phys. Rev.* **139** A1991-A2001.

[59]Sernelius B E, Berggren K F, Jin Z C, Hamberg I and Granqvist C G 1988 Band-Gap Tailoring of Zno by Means of Heavy Al Doping *Phy. Rev. B* **37** 10244-10248.

[60]Mohanty B C, Jo Y H, Yeon D H, Choi I J and Cho Y S 2009 Stress-induced anomalous shift of optical band gap in ZnO:Al thin films *Appl. Phys. Lett.* **95** 062103.

[61]Djurisic A B, Leung Y H, Tam K H, Ding L, Ge W K, Chen H Y and Gwo S 2006 Green, yellow, and orange defect emission from ZnO nanostructures: Influence of excitation wavelength *Appl. Phys. Lett.* **88** 103107.

[62]Djurisic A B, Leung Y H, Tam K H, Hsu Y F, Ding L, Ge W K, Zhong Y C, Wong K S, Chan W K, Tam H L, Cheah K W, Kwok W M and Phillips D L 2007 Defect emissions in ZnO nanostructures *Nanotechnology* **18** 095702.

[63]Ahn C H, Kim Y Y, Kim D C, Mohanta S K and Cho H K 2009 A comparative analysis of deep level emission in ZnO layers deposited by various methods *J. Appl. Phys.***105** 013502.

[64]Xu Z q, Deng H, Li Y and Cheng H 2006 Al-doping effects on structure, electrical and optical properties of c-axis-orientated ZnO:Al thin films *Mater. Sci. Semicond. Process* **9** 132-135.

[65]Grundmann M, Wenckstern H V, Pickenhain R, Nobis T, Rahm A and Lorenz M 2005 Electrical properties of ZnO thin films and optical properties of ZnO-based nanostructures *Superlattices Microstruct.* **38** 317-328.

[66]Xu Q, Hong R D, Huang H L, Zhang Z F, Zhang M K, Chen X P and Wu Z Y 2013 Laser annealing effect on optical and electrical properties of Al doped ZnO films *Opt. Laser Technol.* **45** 513-517.

Table 1. Experimental parameters (number of laser shots and oxygen pressure) used for the pulsed-laser deposition of ZnO and AZO films on Zeonor substrates. The resulting thickness, 2θ angular position, FWHM of the (002) Bragg reflection, value of the *c*-axis length and resistivity are given for each film.

	Sample label	No. of laser shots	Oxygen pressure (mTorr)	Thickness ±error (nm)	2θ (deg)	*c*-parameter (nm)	FWHM (deg)	Resistivity ($10^3 \times$ Ω cm)
ZnO	Z1	5000	75	85±10	34.25	0.5238	0.39	462
	Z2	10000	75	169±22	34.27	0.5235	0.42	17
	Z3	20000	75	340±18	34.34	0.5225	0.44	452
	Z4	5000	150	92±23	34.21	0.5244	0.38	0.15
	Z5	10000	150	190±37	34.23	0.5240	0.41	0.49
	Z6	20000	150	382±74	34.24	0.5240	0.43	17
	Z7	5000	300	97±23	34.21	0.5243	0.38	0.83
	Z8	10000	300	209±43	34.27	0.5235	0.41	22
	Z9	20000	300	422±6	34.26	0.5236	0.41	1.8
AZO	A1	5000	75	67±17	34.34	0.5224	0.52	0.49
	A2	10000	75	131±13	34.40	0.5216	0.52	2.0
	A3	20000	75	263±28	34.45	0.5208	0.49	2.1
	A4	5000	150	74±23	34.40	0.5216	0.49	0.39
	A5	10000	150	140±10	34.48	0.5204	0.49	0.97
	A6	20000	150	289±7	34.46	0.5207	0.46	0.75
	A7	5000	300	86±26	34.48	0.5204	0.70	6.9
	A8	10000	300	199±54	34.48	0.5204	0.66	11
	A9	20000	300	415±4	34.52	0.5198	0.64	21

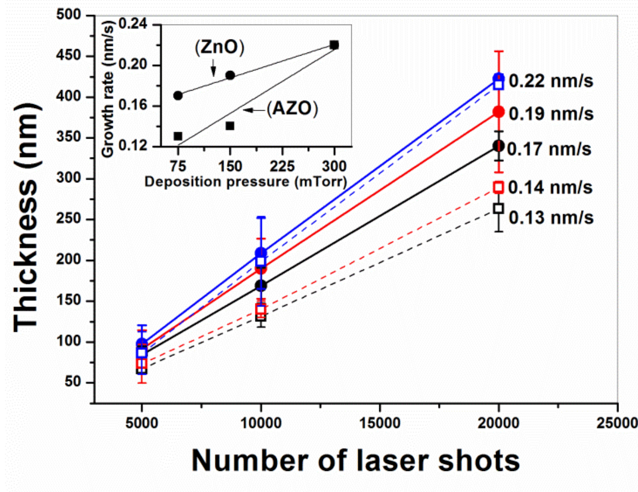

Figure 1. Thickness of ZnO (closed symbols, solid lines) and AZO (open symbols, broken lines) thin films, grown by pulsed-laser deposition, on Zeonor substrates as a function of the number of laser shots (repetition rate 10 Hz) for oxygen ambient pressures of 75 (black), 150 (red) and 300 mTorr (blue). The inset shows the corresponding ZnO and AZO film growth rates (nm/s) as a function of oxygen pressure (mTorr).

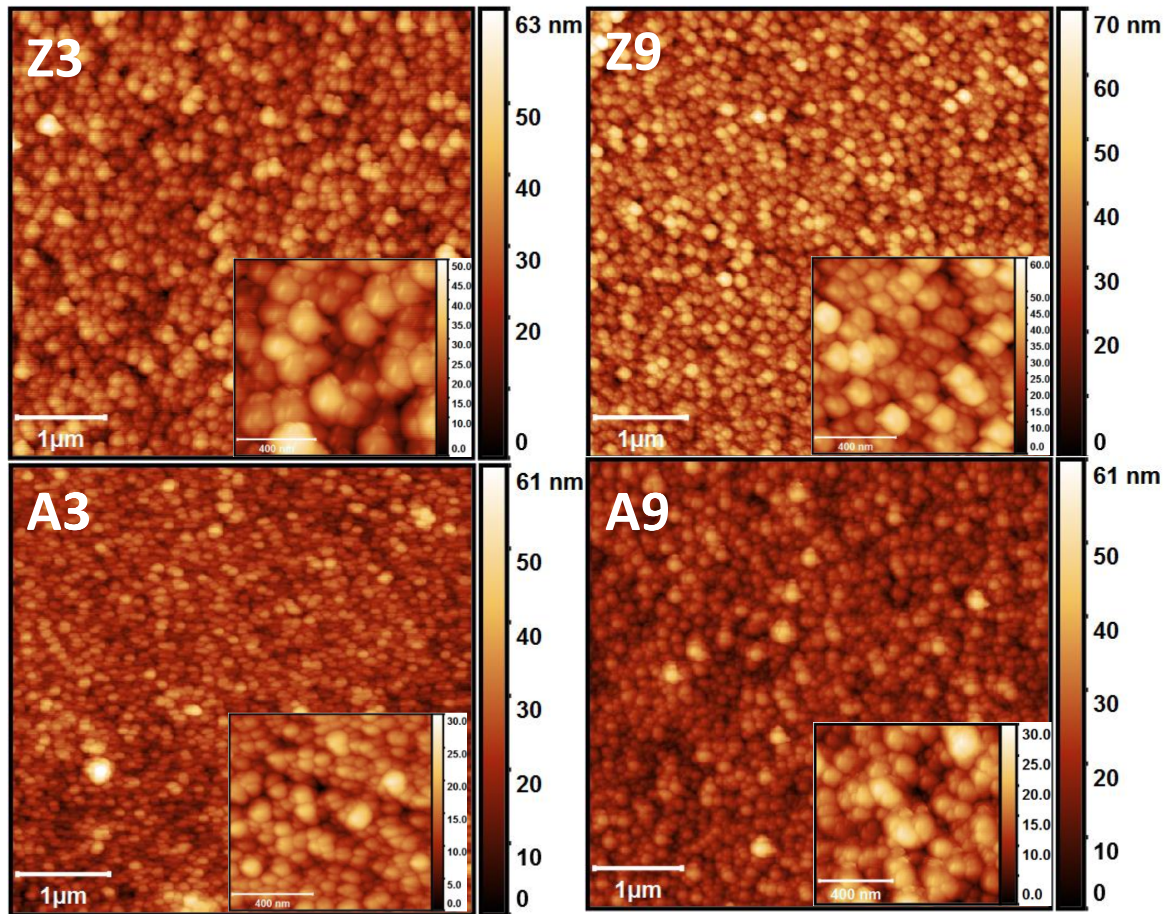

Figure 2. AFM images showing the typical surface topography of a selection of ZnO (upper row) and AZO (lower row) films obtained in this work (samples Z3, Z9, A3 and A9). The films were grown by pulsed-laser deposition on Zeonor substrates using 20,000 laser shots at ambient oxygen pressures of 75 mTorr (left-hand column) and 300 mTorr (right-hand column). The insets show the same surfaces on a more magnified scale to reveal the finer details of the nanostructured grains.

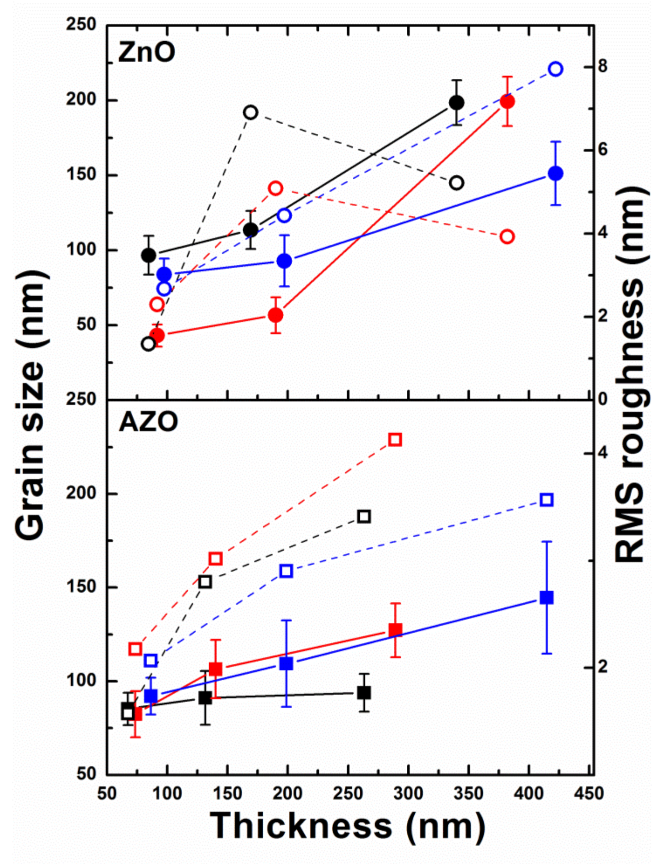

Figure 3. Grain size (closed symbols, solid lines) and rms roughness R_q (open symbols, dashed lines) as a function of film thickness for ZnO and AZO thin films deposited by pulsed-laser on Zeonor substrates at ambient oxygen pressures of 75 (black), 150 (red) and 300 mTorr (blue).

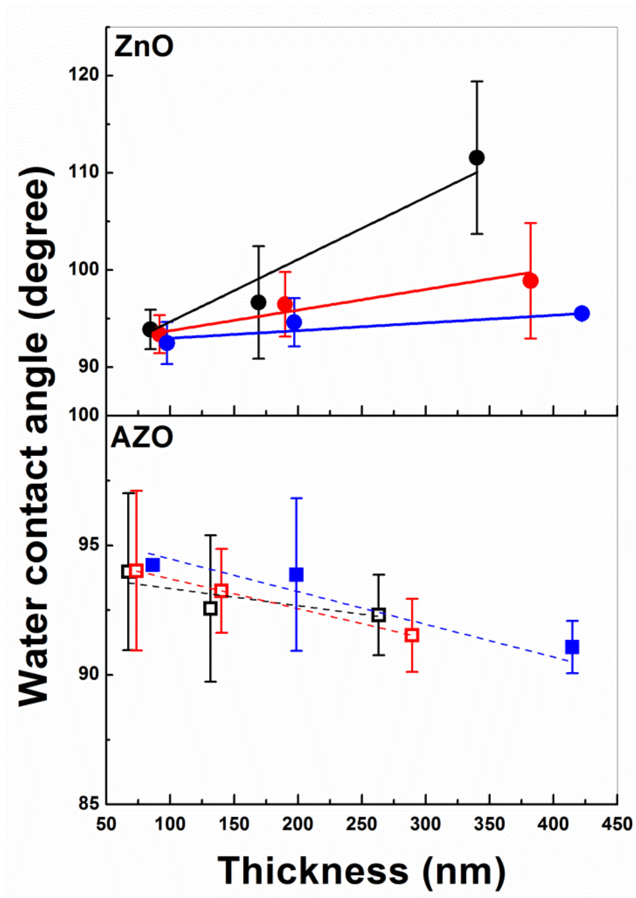

Figure 4. Water contact angle as a function of film thickness for ZnO and AZO thin films deposited by pulsed-laser on Zeonor substrates at ambient oxygen pressures of 75 (black), 150 (red) and 300 mTorr (blue).

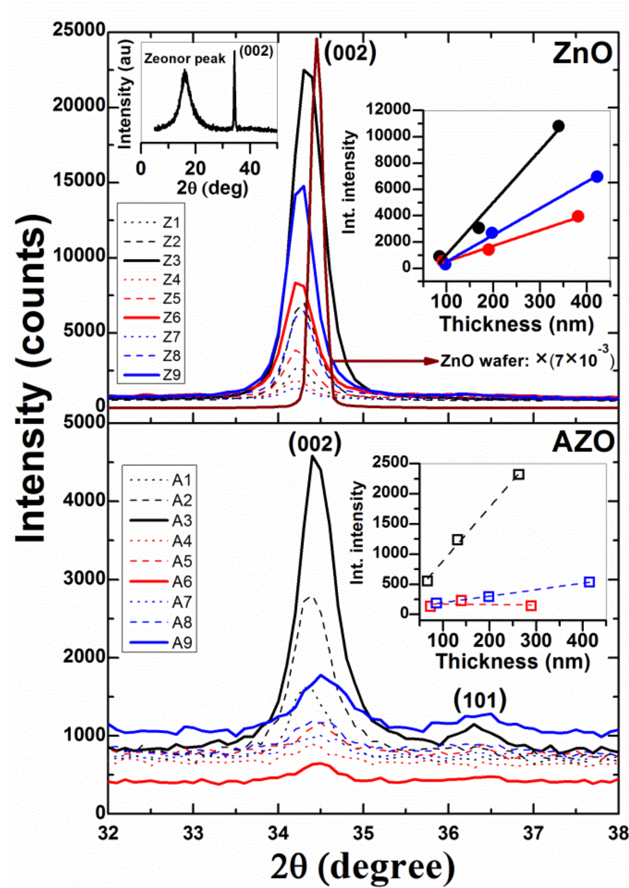

Figure 5. 2θ-ω x-ray diffraction scans for ZnO and AZO thin films deposited by pulsed-laser on Zeonor substrates with 5000 (dotted lines), 10000 (dashed lines) and 20000 (solid lines) laser shots at ambient oxygen pressures of 75 (black), 150 (red) and 300 mTorr (blue). The insets show: (top left) an extended angular range including the amorphous Zeonor diffraction and wurtzite ZnO (002) diffraction peaks; (top and bottom right) the integrated intensities of the (002) peaks as a function of film thickness for the various oxygen pressures used in this work.

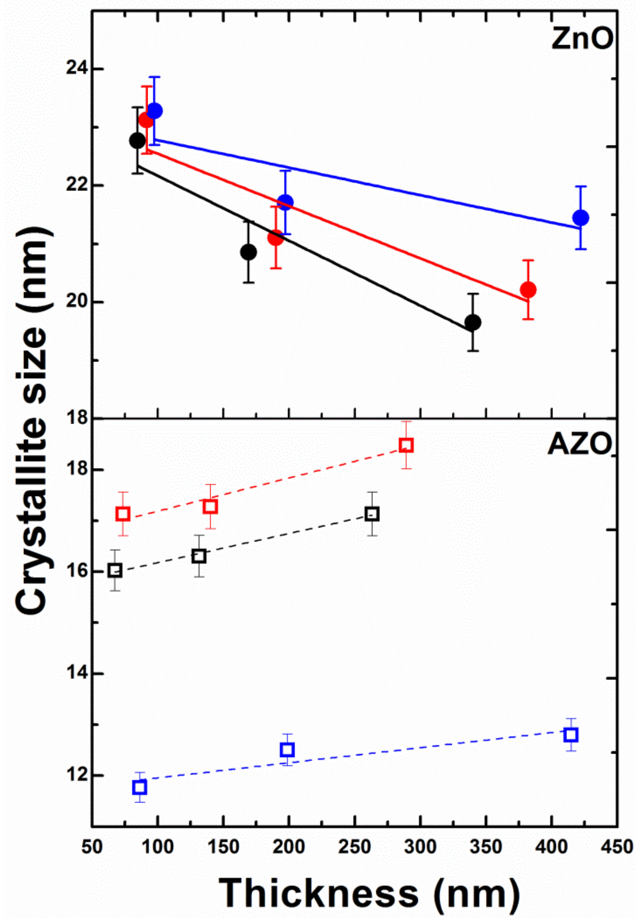

Figure 6. Crystallite size as a function of film thickness for ZnO and AZO thin films deposited by pulsed-laser on Zeonor substrates at ambient oxygen pressures of 75 (black), 150 (red) and 300 mTorr (blue).

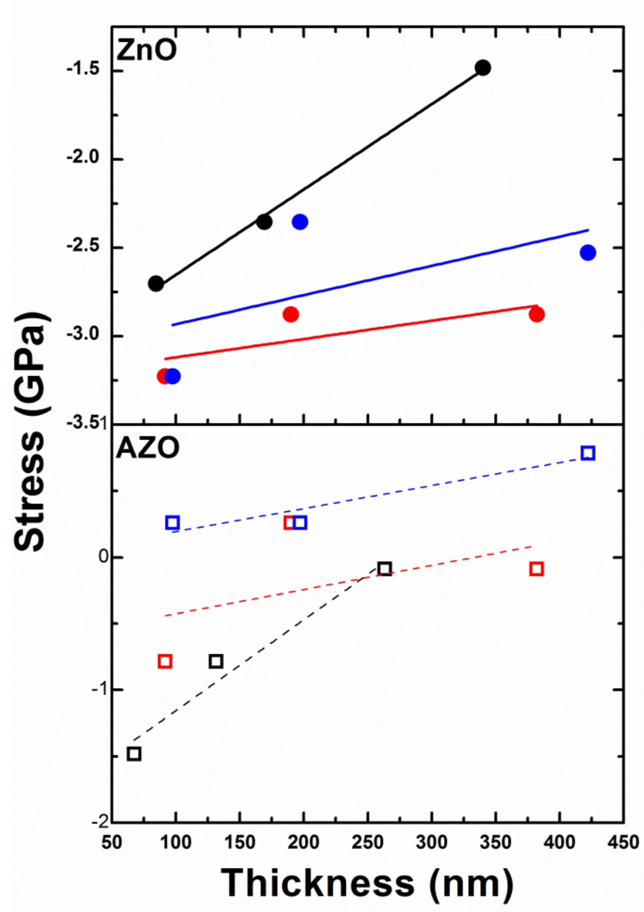

Figure 7. In-plane film stress (GPa) as a function of film thickness for *c*-axis oriented ZnO and AZO thin films deposited by pulsed-laser on Zeonor substrates at ambient oxygen pressures of 75 (black), 150 (red) and 300 mTorr (blue).

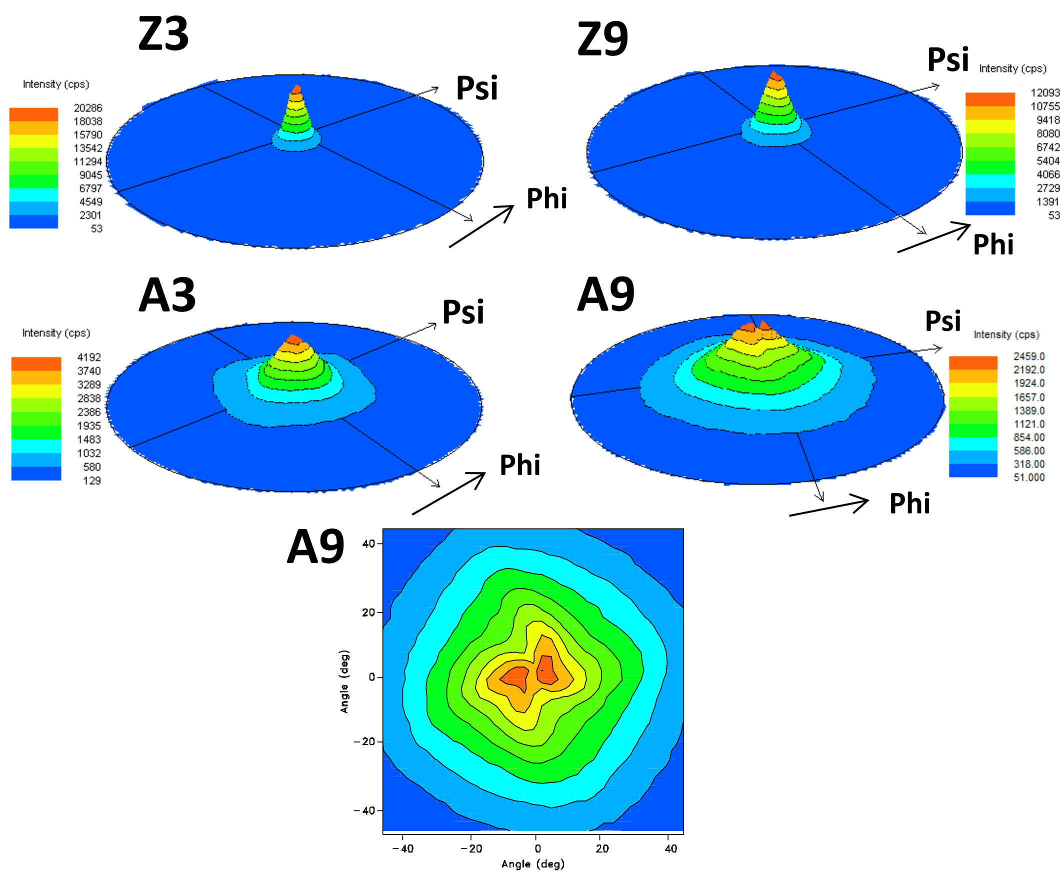

Figure 8. Perspective view of the (002) x-ray pole figure for a selection of ZnO (upper row) and AZO (middle row) films obtained in this work (samples Z3, Z9, A3 and A9). The films were grown by pulsed-laser deposition on Zeonor substrates using 20,000 laser shots at ambient oxygen pressures of 75 mTorr (left-hand column) and 300 mTorr (right-hand column). The psi scale varies between -90° and 90°. The lower panel is a planar projection of the A9 figure on an enlarged psi scale to show the details of the peak splitting.

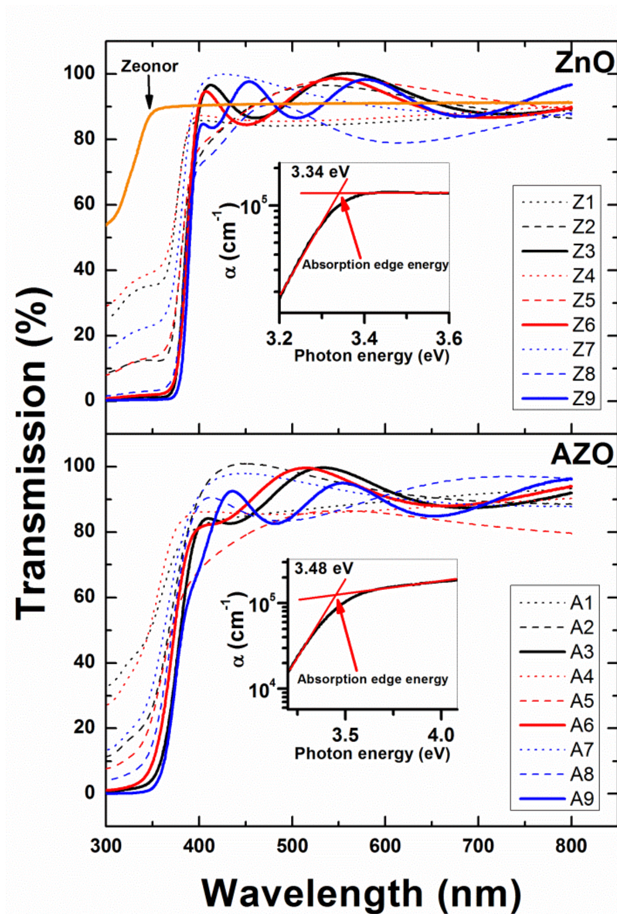

Figure 9. Optical transmission spectrum in the 300 – 800 nm wavelength range for ZnO and AZO thin films deposited by pulsed-laser on Zeonor substrates with 5000 (dotted lines), 10000 (dashed lines) and 20000 (solid lines) laser shots at ambient oxygen pressures of 75 (black), 150 (red) and 300 mTorr (blue). The insets show the absorption coefficient as a function of photon energy in the immediate vicinity of the ZnO (Z3 sample) and AZO (A3 sample) fundamental absorption edges and the graphical method employed in this work to determine the value of the later.

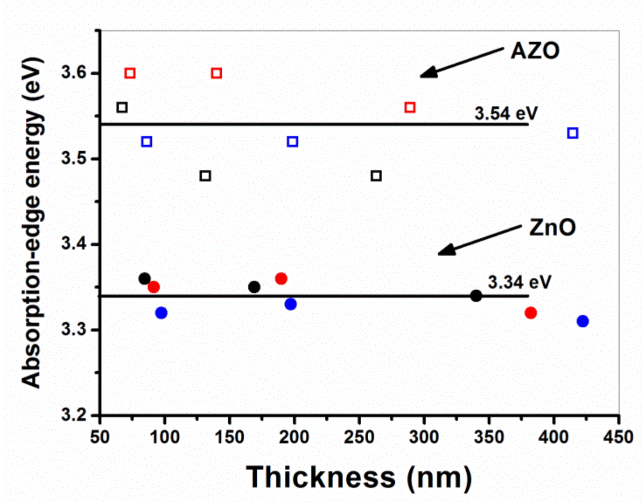

Figure 10. Fundamental absorption edge energy as a function of film thickness for ZnO and AZO thin films deposited by pulsed-laser on Zeonor substrates at ambient oxygen pressures of 75 (black), 150 (red) and 300 mTorr (blue).

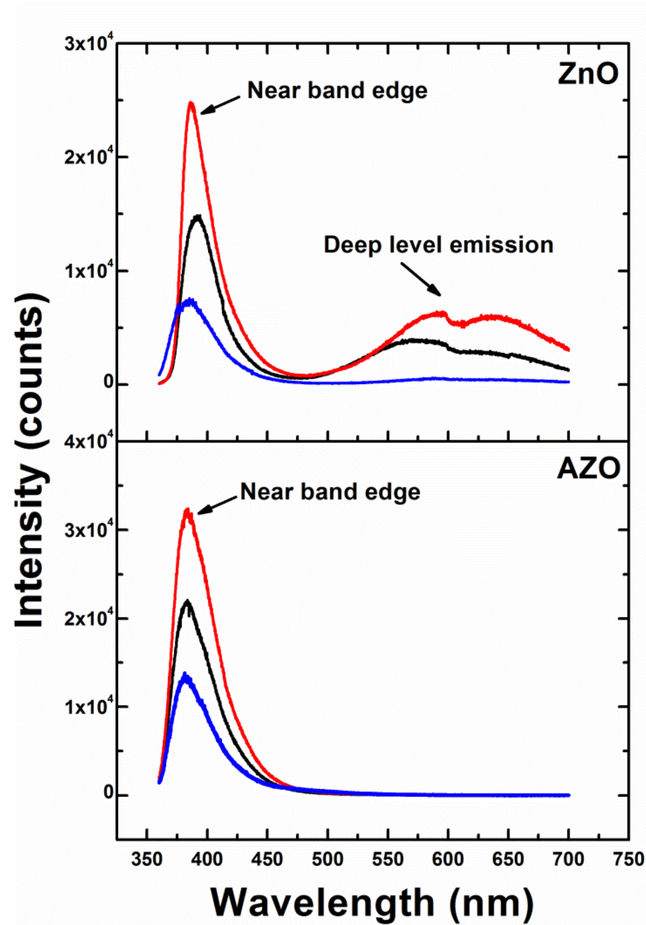

Figure 11. Low temperature (13 K) photoluminescence spectrum for ZnO and AZO thin films deposited by pulsed-laser with 20000 laser shots on Zeonor substrates at ambient oxygen pressures of 75 (black), 150 (red) and 300 mTorr (blue).

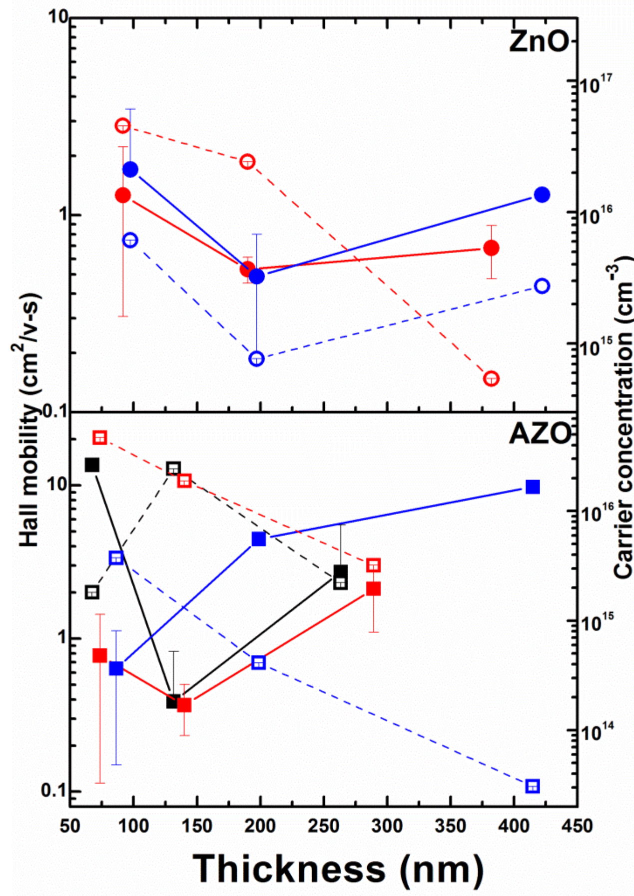

Figure 12. Hall mobility (closed symbols, solid lines) and carrier concentration (open symbols, dashed lines) as a function of film thickness for ZnO and AZO thin films deposited by pulsed-laser on Zeonor substrates at ambient oxygen pressures of 75 (black), 150 (red) and 300 mTorr (blue).